Biophysical Journal, Vol. 99

Supporting Material

Deformation of dynamin helices damped by membrane friction

Sandrine Morlot, Martin Lenz, Jacques Prost, Jean-François Joanny, and Aurélien Roux

Deformation of dynamin helices damped by membrane friction
Supporting Material

S1 Supporting theoretical analysis

S1.1 Screening of rotation by bare membrane sections

Here we discuss the consequences of the presence of a hypothetical break in the helix. If the break is very short, the resulting bare membrane region is still able to transmit torques thanks to its membrane viscosity, and therefore the break is not evident in the measurements presented in Fig. 2 of the main text. Longer breaks, however, result in a mechanical discontinuity of the tube and would therefore have noticeable consequences on bead rotation.

Let us consider a tube with a dynamin coat disassembled between two altitudes z_1 and z_2. In that case, it is difficult for the piece of helix between 0 and z_1 to drag the piece between z_2 and L along, as the mechanical connection between the two is only realized through a section of bare membrane tubule. In order to assess the range of this mechanical connection, we consider an infinite membrane tubule covered by dynamin only up to the altitude z_1. We denoting by $\Omega(z)$ the rotation velocity of the membrane tubule and the water it encloses at altitude $z \in [z_1, +\infty]$. It is easily shown that the upward flux of angular momentum transmitted through the water within the tubule at altitude z is equal to $\frac{\pi}{2}\eta r^4 \partial_z \Omega$. The angular momentum transmitted by the membrane is $2\pi r^3 \eta_m \partial_z \Omega$, where $\eta_m \simeq 10^{-9}\mathrm{kg.m^{-1}.s^{-1}}$ is a typical membrane viscosity (1). Meanwhile, the surrounding fluid exerts a friction on the tubule. It thus acts as a momentum drain and sucks an amount $2\pi\eta r^2\Omega$ of angular momentum per unit length per unit time (this expression assumes that the length scale ℓ over which Ω varies is much larger than r). Writing the conservation of angular momentum along the membrane tubule, we conclude that its rotational velocity decays as $\Omega(z) = \Omega(z_1)\exp\left[-(z-z_1)/\ell\right]$, where $\ell = \frac{r}{2}\sqrt{1+4\frac{\eta_m}{\eta r}} \simeq \sqrt{\frac{r\eta_m}{\eta}} \simeq 100\,\mathrm{nm} \gg r$. Therefore, friction of the membrane with the surrounding fluid screens the tube's rotation over length scales of order ℓ. This means that disassembling the helix over a patch of size $\approx 100\,\mathrm{nm}$ would be enough to spoil the linear relationship observed in Fig. 2(a), as well as the sinusoidal profile of Fig. 2(c). From this we deduce that if any helix discontinuities are present in our experiments, they must be few and much smaller than 100 nm.

S1.2 Bead rotation is not due to unbraiding

It has been suggested in Ref. (2) that bead rotation in experiments similar to ours (3) is due to the unwinding of a braid formed by two tubes attached at $z = 0$ and $z = L$ respectively—here we refer to those as tubes 1 and 2. Within this hypothesis, a bead attached to tube 1 in the vicinity of $z = 0$ should rotate by only a modest amount, as it is close to the tube attachment point. Statistically, about half of the beads in this region should be bound to tube 2. These are expected to rotate by a large amount, comparable to those located in $z = L$ in Fig. 2(a) of the main text. That no such dispersion is observed in our data is proof that we monitor the rotation of a single tube.

S1.3 Thermodynamic description of the membrane reservoir

In order to predict the dynamics of a tube as in Fig. 3 of the main text, the diffusion equation Eq. (5) of the main text [or more generally Eq. (21) of Ref. (4)] must be supplemented with boundary conditions. Ref. (4) proposes the boundary condition $\delta\mu_e(z=0)=\delta\mu_e(z=L)=0$, where $z=0$ and $z=L$ correspond to the extremities of the tube. This is meant to describe contact of the tube with two reservoir: one of membrane and one of helix. Although the former is perfectly legitimate in our experimental setting, interpreting the latter is somewhat more difficult. Moreover, using this boundary condition leads to very strongly bent and stretched membrane profiles [Eq. (45) and Fig. 3 of Ref. (4)]. These profiles suggest that the membrane should break much sooner than is actually observed (5), and are somewhat at odds with the physical intuition that the membrane should relax to a weakly bent, low-energy configuration at long times.

In this section we propose a more satisfactory set of boundary conditions by properly describing the contact of the tube with membrane-only reservoirs in $z=0$ and $z=L$. Denoting by

$$\delta\mu = \left.\frac{\partial f}{\partial \rho}\right|_{u_{z\theta},\Phi} \tag{S1}$$

the tube total chemical potential, the Gibbs-Duhem relation reads

$$\mathrm{d}(\delta\mu) = \frac{\mathrm{d}(\delta\mathfrak{p})}{\rho} + \delta\mu_e \mathrm{d}(\delta\Phi) + \frac{\delta h}{\rho}\mathrm{d}(\delta u_{z\theta}). \tag{S2}$$

As the two last terms in the right-hand side are of second order in δ (defined in the main text), we neglect them in the following. The chemical potential is defined up to a constant, which we choose such that $\delta\mu=0$ in the reference state (hence the δ in $\delta\mu$). Contact with a membrane reservoir fixes the membrane chemical potential, which is defined as

$$\mu_m = \left.\frac{\partial f}{\partial \rho_m}\right|_{\rho_h,u_{z\theta}}, \tag{S3}$$

where $\rho_h=\rho\Phi$ and $\rho_m=\rho(1-\Phi)$ are the mass densities of helix and membrane, respectively. Eqs. **S1**, **S3** and the definition of $\delta\mu_e$ [see Eq. (3) of the main text] imply that $\mu_m=\delta\mu-\Phi\delta\mu_e$. Because of the convention chosen above, $\delta\mu$ vanishes in the reference state. According to its definition, so does $\delta\mu_e$. Therefore $\delta\mu=\delta\mu_e=0$ in contact with the reservoir. Since the definition of the reference state assumes that the tube is in equilibrium with the reservoir, we deduce from this that equilibrium with the membrane reservoir is expressed by the condition $\mu_m=0$, and we can thus write $\mu_m=\delta\mu_m$.

Integrating Eq. (S2) to first order in δ yields $\delta\mu=\delta\mathfrak{p}/\rho$, and so $\delta\mu_m=0=\delta\mathfrak{p}/\rho-\Phi\delta\mu_e$. Combining this with Eqs. **4a** and **4b**[1], the boundary conditions are expressed by the fact that the reactive forces $\delta\mathfrak{p}(z=0 \text{ or } z=L,t)$, $\delta h(z=0 \text{ or } z=L,t)$ and $\delta\mu_e(z=0 \text{ or } z=L,t)$ in contact with the membrane reservoirs are respectively equal to

$$\delta\mathfrak{p}^r = \sigma_{\mathrm{ext}} + \frac{\tau_{\mathrm{ext}}}{p} - \left(\tilde{\xi}_z\Delta\mu + \frac{\tilde{\xi}_\theta\Delta\mu}{p}\right) \tag{S4a}$$

$$\delta h^r = -\tau_{\mathrm{ext}} + \tilde{\xi}_\theta\Delta\mu \tag{S4b}$$

$$\delta\mu_e^r = \frac{\sigma_{\mathrm{ext}}}{\rho\Phi} + \frac{\tau_{\mathrm{ext}}}{\rho\Phi p} - \left(\frac{\tilde{\xi}_z\Delta\mu}{\rho\Phi} + \frac{\tilde{\xi}_\theta\Delta\mu}{\rho\Phi p}\right), \tag{S4c}$$

[1] In the more general case where the two first modes of the tube are not ignored, this equation should be combined with Eqs. (19a) and (19b) of Ref. (4). Noting that the terms with z-derivatives in these equations are vanishingly small in the hydrodynamic limit, this yields the same result as the one presented here.

where we use the fact that the tube's tension and torque at its endpoints are equal to the externally applied force and torque $\sigma_{\rm ext}$ and $\tau_{\rm ext}$. Combining Eq. (21) of Ref. (4) and Eqs. **S4** with the initial condition $(\delta\rho, \delta u_{z\theta}, \delta\Phi)(z, t = 0) = (0, 0, 0)$, we compute the tube's full relaxation dynamics in the case $\sigma_{\rm ext} = 0$, $\tau_{\rm ext} = 0$, which yields the results presented in Fig. 3 of the main text. As in Ref. (4), the values of the active terms are chosen to reproduce the changes of pitch and radius observed in electron microscopy (6), which reads

$$\tilde{\xi}_z \Delta\mu \simeq -3.5 \times 10^{-11}\,\mathrm{N} \quad \text{and} \quad \tilde{\xi}_\theta \Delta\mu \simeq 2.6 \times 10^{-17}\,\mathrm{N.m.} \tag{S5}$$

Note that this new description yields a negative $\tilde{\xi}_z \Delta\mu$, as opposed to the positive $\tilde{\xi}_z \Delta\mu$ calculated in Ref. (4). This means that we now predict that the tube tends to contract upon GTP hydrolysis, whereas a positive $\tilde{\xi}_z \Delta\mu$ implies an extension. Our new description, unlike that of Ref. (4), is therefore in agreement with the experimental observations of Ref. (3) and the main text.

S1.4 Long-time dynamics of a tube attached at both ends

In this paragraph we discuss the possibility for a continuous tube attached to the glass in two points (and therefore prevented from rotating) to induce bead rotation. Assuming a continuous helix whose axis is a straight line throughout the dynamics, no such motion seems possible, and indeed none is expected from our formalism. In order to show this we consider a tube whose initial state is described by $\delta u_{z\theta}(z, t = 0) = 0$. As discussed in the main text and the previous section, the final state has a uniform tension σ and torque τ, as well as a uniform membrane chemical potential, which implies $\delta u_{z\theta}(z, t = +\infty) = \text{constant}$. Moreover, the fact that the helix is held in $z = 0$ and $z = L$ implies

$$[\theta(L, +\infty) - \theta(L, 0)] - [\theta(0, +\infty) - \theta(0, 0)] = \delta u_{z\theta}(z, +\infty) L = 0, \tag{S6}$$

hence $\delta u_{z\theta}(z, +\infty) = 0$ and the tube does not undergo any rotation.

Rotation of a tube bound at its two ends is however observed in Fig. 2(c), and is found to yield a sinusoidal velocity profile. Here we propose a possible explanation for this observation. Because of the propensity of the helix to rotate, torques build up in the tube following GTP injection, and have been observed to lead to supercoiling of the tube (3, 6). The formation of a supercoil from a stressed rod is a local phenomenon, which does not require an overall rotation of the rod or flow of membrane. Consequently, we expect supercoils to form quickly (on non-hydrodynamic time scales) following the GTP-induced build-up of torque. To simplify, let us assume that the formation of these supercoils is irreversible—once formed they are thus "frozen" for the rest of the dynamics. Supercoil formation leads to a local relaxation of the tube, and therefore we expect that the helix in the vicinity of the supercoils will change its pitch and radius to some extent. This creates an inhomogeneous initial condition for the tube's hydrodynamic relaxation. As a consequence, and unlike in the case considered above, $\delta u_{z\theta}(z, t = 0)$ is not equal to zero everywhere. The precise structure of this initial condition depends on the details of the supercoiling mechanism, and is beyond the scope of this study. Assuming however that no additional supercoiling occurs on hydrodynamic time scales, we predict that this initial condition relaxes according to the diffusion equation Eq. (5). Since the now complicated function $\delta u_{z\theta}(z, t = 0)$ generically has a non-vanishing projection onto the slowest mode of the diffusion equation, we expect that the long-time dynamics of the tube is dominated by the sinusoidal profile observed in Fig. **2**(c).

Note that the mechanism presented here might not be the only possible explanation for this phenomenon, and is only meant as an illustration of the fact that rotation in a tube bound at its two ends is not logically forbidden. Moreover, it illustrates the general feature that if the paradox

proposed here is indeed resolved through local, microscopic relaxation processes, then the form of long-time relaxation of the tube is not affected and we expect our hydrodynamic predictions to hold.

References

1. Dimova, R., B. Pouligny, and C. Dietrich, 2000. Pretransitional effects in dimyristoylphosphatidylcholine vesicle membranes: optical dynamometry study. *Biophys. J.* 79:340–356.

2. Pucadyil, T. J., and S. L. Schmid, 2008. Real-time visualization of dynamin-catalyzed membrane fission and vesicle release. *Cell* 135:1263–1275.

3. Roux, A., K. Uyhazi, A. Frost, and P. De Camilli, 2006. GTP-dependent twisting of dynamin implicates constriction and tension in membrane fission. *Nature (London)* 441:528–531.

4. Lenz, M., J. Prost, and J.-F. Joanny, 2008. Mechanochemical action of the dynamin protein. *Phys. Rev. E* 78:011911.

5. Kozlov, M. M., 1999. Dynamin: Possible mechanism of "pinchase" action. *Biophys. J.* 77:604–616.

6. Danino, D., K.-H. Moon, and J. E. Hinshaw, 2004. Rapid constriction of lipid bilayers by the mechanochemical enzyme dynamin. *J. Struct. Biol.* 147:259–267.

S2 Supporting movies—legends

S2.1 Supporting movie 1

Experimental movie corresponding to Fig. 1(b). See main text for legend.

S2.2 Supporting movie 2

Illustration of the dynamics presented in Fig. 3 of the main text. Only a few helical turns are shown, and in this small region the deformation looks spatially homogeneous—it however has a more complicated spatial structure on larger length scales, as discussed in the main text and in Ref. (4). The movie displays the asymptotically exponential relaxation of the helix's three hydrodynamic modes. The relaxation times involved in a real system are well separated and range from hundreds of microseconds to seconds (see Fig. 3). Here these time scales are modified for easier visualization. Each of the three modes therefore appears to have a relaxation time equal to 0.4 s. Note that the amplitude of the first mode is very small compared to the next two and might therefore escape the reader's attention on first viewing. Finally, the model used allows for both bending and stretching of the membrane (4). Although its amplitude is small, the former induces some bulging of the membrane visible in this movie. The membrane is represented as a semi-transparent surface, and its transparency is proportional to its stretching ratio.

S3 Supporting figures

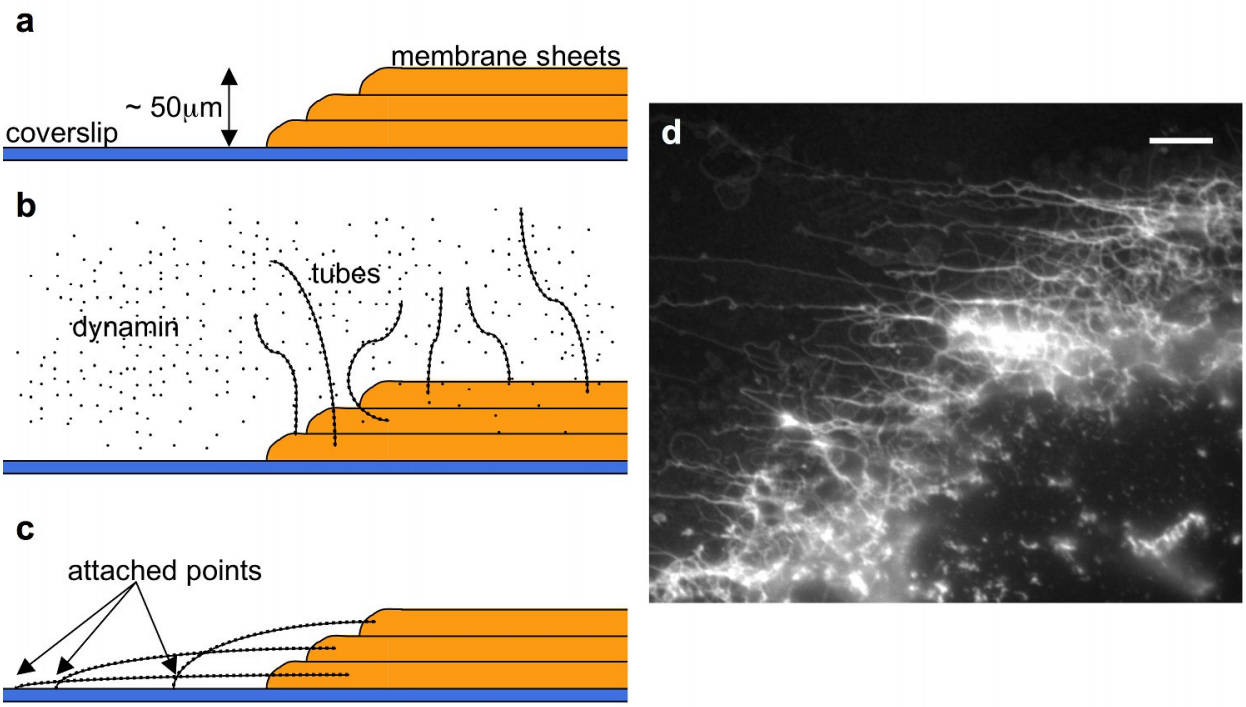

Figure S1: Geometry of the membrane sheets assay. (a-c) Side-view schematics representing (a) the membrane sheets after rehydration and before dynamin injection, (b) the appearance of dynamin-coated tubes on membrane sheets after dynamin injection, and (c) tubes bound to the coverslip following dynamin injection. Note that the tubes represented here are essentially parallel to the coverslip, enabling us to monitor their dynamics, but are some distance away from it, thus allowing the beads to rotate freely. (d) Top-view fluorescence microscopy image of a membrane sheet at the stage represented in (c) (dynamin is fluorescently labeled). Scale bar, 5 μm.

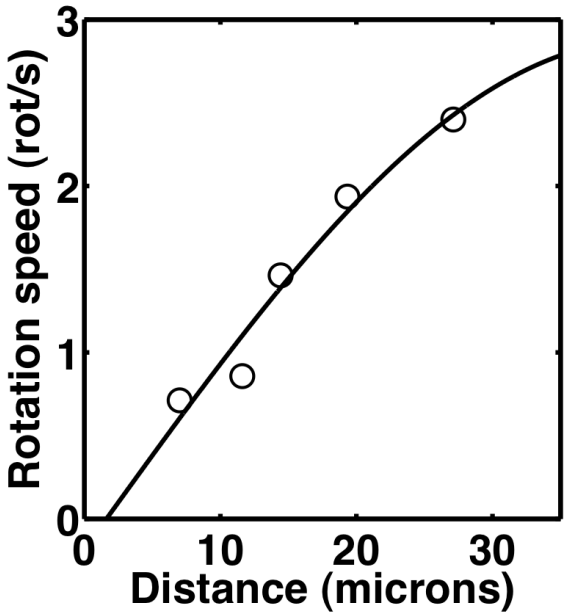

Figure S2: Experimental determination of the boundary conditions for a tube bound at one end only. In order to calculate the maximum wavelength $\lambda_{\max}$ compatible with the boundary conditions of a given tube, we assume that tubes visibly bound to the glass at both ends obey the boundary conditions $\delta\theta(z = 0, t) = \delta\theta(z = L, t) = 0$, which yields $\lambda_{\max} = 2L$. Fig. 2(c) of the main text demonstrates the validity of this description, as it shows that the best sinusoidal fit to the bead velocity data coincides with the boundary conditions directly assessed from video microscopy data. For tubes bound in $z = 0$ and free to rotate in $z = L$, we assume $\delta\theta(z = 0, t) = 0$ and $\partial_z\delta\theta(z = L, t) = 0$, where the latter condition corresponds to a zero torque being applied to the tube in $z = L$. This implies $\lambda_{\max} = 4L$. In this figure we present experimental data (circles) similar to that of Fig. 2(c) for such a tube, as well as the best sinusoidal fit of the form $\Omega = \Omega_0 \sin[2\pi(z - z_0)/\lambda_{\max}]$ for this data (line), where Ω_0, z_0 and $\lambda_{\max}$ are adjustable parameters. The sinusoidal fit yields $\lambda_{\max} \simeq 160\,\mu$m, consistent with the direct measurement $L \simeq 45\,\mu$m. Note that no beads are attached to the vicinity of the end of this tube, and therefore no data was collected in the region $z > 30\,\mu$m. Moreover, the fit places the tube's origin within $2\,\mu$m of the directly observed attachment point ($z_0 = 1.6\,\mu$m). This shows that a sinusoid with $\lambda_{\max} = 4L$ is a good description of a tube bound at one end only, and validates the use of this condition in constructing Fig. 2(d).

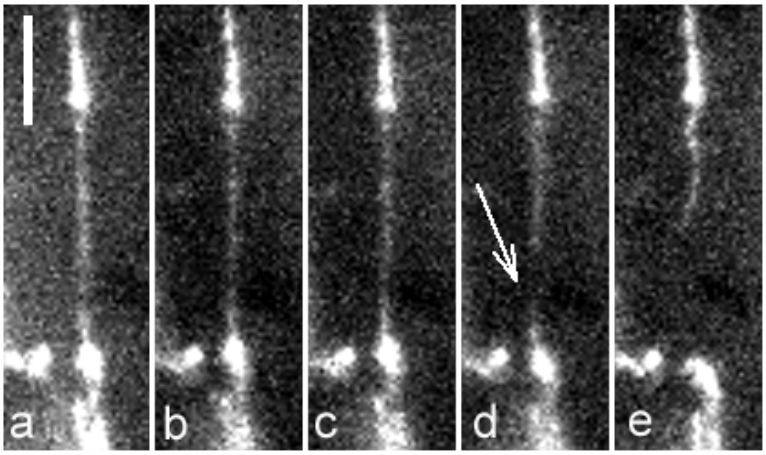

Figure S3: Direct epifluorescence observation of an Alexa-488–dynamin polymer [prepared as in Ref. (3)] during GTP hydrolysis using an EMCCD Andor camera. (a) tube anchored at both ends after injection of 6.3 μM fluorescently labeled dynamin on membrane sheets and before GTP injection. (b) 12.74 s after injection of 100 μM GTP. (c) 13.33 s after GTP injection. (d) Fission occurs (white arrow) 13.93 s after GTP injection. (e) 15.11 s after GTP injection and 1.18 s after tube fission. As mentioned in the main text, no significant discontinuity of the dynamin helix is observed during this experiment apart from the main breaking event. This is evidence that the dynamin coat remains continuous up until tube breaking. Scale bar: 5 μm.

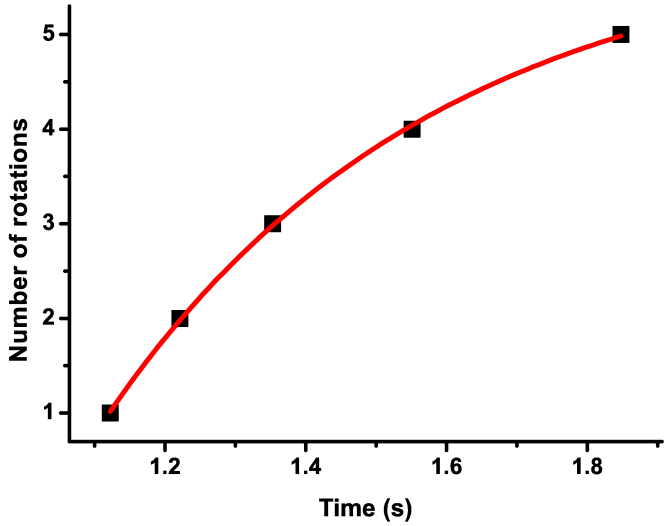

Figure S4: Fit procedure for the relaxation times presented in Fig. 2(d) of the main text. Relaxation times are deduced from the data points representing the number of turns $\theta/2\pi$ of a specific bead as a function of time t (black squares). Ignoring the initial phase where GTP injection and short wavelength modes interfere with the tube relaxation, these curves are fitted with the function $\theta/2\pi = a\exp(-t/\tau) + b$ in the Origin 8.1 software (red line), where a, b and τ are adjustable parameters. The optimal value for τ is the relaxation time plotted in Fig. 2(d).